fractal and fractional

MDPI

Article

Finite-Time Synchronization and Mittag–Leffler Synchronization for Uncertain Fractional-Order Delayed Cellular Neural Networks with Fuzzy Operators via Nonlinear Adaptive Control

Hongguang Fan [1,2,3], Kaibo Shi [4], Zizhao Guo [5,*], Anran Zhou [1,2] and Jiayi Cai [6]

[1] College of Computer, Chengdu University, Chengdu 610106, China; fanhongguang@cdu.edu.cn (H.F.); zhouanran@cdu.edu.cn (A.Z.)
[2] Key Laboratory of Digital Innovation of Tianfu Culture, Sichuan Provincial Department of Culture and Tourism, Chengdu 610106, China
[3] Engineering Research Center for Big Data Application in Private Health Medicine of Fujian Universities, Putian University, Putian 351100, China
[4] School of Electronic Information and Electrical Engineering, Chengdu University, Chengdu 610106, China; shikaibo@cdu.edu.cn
[5] Shenzhen Institute for Advanced Study, University of Electronic Science and Technology of China, Shenzhen 610056, China
[6] School of Mathematics and Statistics, Guizhou University of Finance and Economics, Guiyang 550025, China; caijiayi2018@email.szu.edu.cn
* Correspondence: guozz25@uestc.edu.cn

Abstract

This paper investigates a class of uncertain fractional-order delayed cellular neural networks (UFODCNNs) with fuzzy operators and nonlinear activations. Both fuzzy AND and fuzzy OR are considered, which help to improve the robustness of the model when dealing with various uncertain problems. To achieve the finite-time (FT) synchronization and Mittag–Leffler synchronization of the concerned neural networks (NNs), a nonlinear adaptive controller consisting of three information feedback modules is devised, and each submodule performs its function based on current or delayed historical information. Based on the fractional-order comparison theorem, the Lyapunov function, and the adaptive control scheme, new FT synchronization and Mittag–Leffler synchronization criteria for the UFODCNNs are derived. Unlike previous feedback controllers, the control strategy proposed in this article can adaptively adjust the strength of the information feedback, and partial parameters only need to satisfy inequality constraints within a local time interval, which shows our control mechanism has a significant advantage in conservatism. The experimental results show that our mean synchronization time and variance are 11.397% and 12.5% lower than the second-ranked controllers, respectively.

Keywords: adaptive parameter; synchronization pattern; fuzzy rule; neural network; fractional-order

Academic Editors: Ying Luo, Necdet Sinan Özbek and Yangquan Chen

Received: 29 July 2025
Revised: 22 September 2025
Accepted: 26 September 2025
Published: 29 September 2025

Citation: Fan, H.; Shi, K.; Guo, Z.; Zhou, A.; Cai, J. Finite-Time Synchronization and Mittag–Leffler Synchronization for Uncertain Fractional-Order Delayed Cellular Neural Networks with Fuzzy Operators via Nonlinear Adaptive Control. *Fractal Fract.* **2025**, *9*, 634. https://doi.org/10.3390/fractalfract9100634

1. Introduction

In recent years, people's work and lives have been inextricably linked to various complex networks and NNs [1,2]. For example, urban public transportation networks, energy and power systems, information transmission networks, online social networks, and deep learning networks have dramatically changed all aspects of people [3,4]. NNs of varying distinctiveness have been widely utilized in signal processing, cooperative control, system stability, dynamics analysis, and other fields [5–8]. Synchronization, as

an important aggregation behavior of NNs, inevitably becomes a cutting-edge direction for researchers [9]. Synchronized neuronal firing plays an important role in cognitive function by enhancing the processing of specific sensory information, thereby improving concentration. Fireflies flashing in nature, birds flying in flocks, and crickets chirping in unison show the importance of synchronized behavior to the life of biota [10,11]. Up to the present, various synchronization patterns have emerged, including complete synchronization [12], impulsive synchronization [13], exponential synchronization [14], Mittag–Leffler synchronization [15], and finite-time synchronization [16].

Few NNs can achieve synchronization consistency without the aid of external control. To finish various synchronization tasks for NNs, there exist many control strategies, such as PID control [17–21], sampled-data control [22], event-triggered control [23], feedback control [24], and adaptive control [25]. In [26], the global synchronization of NNs was investigated through feedback control of a few key nodes. The authors of [27] conducted the asymptotic synchronization of delayed networks with uncertainties under feedback control at partial discrete instants. By concise control schemes and solution formulas, Hua et al. [28] derived the sufficient synchronization conditions of NNs with multi-link frameworks and multiple delays. In [29], Wan et al. studied the master–slave synchronization of delayed network systems by using the Barbalat lemma and adaptive control. An adaptive feedback controller was designed for the global synchronization of quaternion NNs in [30] to reduce the control cost and conservatism.

Compared to integer-order calculus, fractional-order calculus can more accurately describe the dynamic changes of actual systems due to its infinite memory and genetic characterizations [31,32]. The advantages of fractional calculus make it successfully applied in various engineering and biophysical fields [33]. For instance, the stress relaxation and creep behavior of materials such as soil and asphalt can be more accurately captured by fractional-order differential constitutive models, which are more concise and effective than integer-order models [34]. Many scholars have introduced fractional calculus into network modeling and studied the synchronization control of fractional NNs [35–37]. In [38], Xiao et al. solved the FT synchronization of fractional delayed BAM NNs by using a linear feedback controller. In [39], Popa et al. analyzed the Mittag–Leffler master–slave synchronization problem for fractional NNs with hybrid delays via state feedback schemes. Using feedback control methods, the authors derived the flexible synchronization criteria and the Mittag–Leffler synchronization of fractional fuzzy NNs [40,41].

The dynamic behavior of NNs often manifests as strong nonlinearity, time variation, and inaccuracy measurements [42]. For a biological neural network, a neuron receives input signals from thousands of synapses. It does not simply add up all the input values linearly. The neuron's state response is more akin to a nonlinear threshold decision-making process [43]. Fuzzy logic operators provide just the right mathematical framework to express this nonlinear integration [44]. For example, Li and Cao et al. [45] aimed to probe a class of memristive NNs with different fuzzy operators. In [46], the synchronization of discontinuous delayed neural networks with fuzzy AND and fuzzy OR was discussed using adaptive control schemes. Based on nonlinear feedback control methods, the global synchronization and the FT synchronization of fuzzy network systems with delays were discussed in [47,48].

In addition to fuzziness, the dynamic behavior evolution of NNs is often accompanied by uncertainties at the same time. In [49], Ansari et al. investigated the FT synchronization for fractional quaternion-valued NNs by the desired sliding motion. In [50], Chen et al. obtained the synchronization conditions of discontinuous T-S fuzzy NNs with system uncertainties under a fuzzy feedback controller. The FT synchronization of fuzzy cellular NNs with uncertainties and the FT Mittag–Leffler synchronization of Caputo fractional

memristive systems were considered in [51,52]. However, few works have investigated both FT synchronization and FT Mittag–Leffler synchronization of fractional fuzzy NNs with time delays and system uncertainties through nonlinear adaptive control and feedback control schemes. Compared to the PID control [17,18] and the fixed gain feedback control [16,50–52], we adopt adaptive gain feedback control, which reduces control time by adjusting its control strength in real time, ensuring the robustness of the controller under uncertain parameters. The design of the control law and parameter update law works together to ensure the negative definiteness of the Lyapunov function. The experimental results show that our controller saves at least 11.397% control time compared with the related controllers. The primary challenge of this paper is to design energy-efficient adaptive controllers for synchronization tasks when parameters are only within a local time interval.

Sparked by the above discussions, we study the adaptive FT synchronization and Mittag–Leffler synchronization for fuzzy UFODCNNs. The main contributions of this article lie in three points. First, we give a general fractional-order fuzzy model, which includes uncertainties and delays, and nonlinear activation functions. Second, neuroendocrine PID controllers [20] and BELBIC PID controllers [21] focus on set-point regulation or non-delayed systems, lacking direct compensation mechanisms for time-delayed systems. The fixed-gain feedback controllers in [16,50–52] do not have adaptive adjustment mechanisms. Compared with these existing control schemes, we design an adaptive nonlinear feedback controller consisting of three information feedback modules, and each submodule performs its function based on current and delayed historical information. Third, novel FT synchronization and FT Mittag–Leffler synchronization conditions for fuzzy UFODCNNs can be achieved based on the fractional comparison theorem and the adaptive controller. Different from the parameters in [44–47] satisfying inequality constraints from the initial moment to the current moment, the partial system parameters of our work only need to satisfy inequality constraints within a local time interval $[\underline{t}, \bar{t}\,]$. Our control method can be used for synchronization analysis of fractional-order delayed memristive NNs and can also be applied to the FT consistency control of multi-agent systems. The FT synchronization results obtained in this article can be considered for the image information encryption and decryption within the scheduled time.

We use the following notations. $\mathbb{N}_1^k = \{1, 2, \cdots, k\}$. $\mathbb{R}$ is the set of real numbers. $\mathbb{C}^1([t_0, +\infty), \mathbb{R})$ is the set of continuous differential functions from $[t_0, +\infty)$ into $\mathbb{R}$. ${}_{t_0}^{c}\mathscr{D}_t^{\alpha}\eta(t)$ and ${}_{t_0}I_t^{\alpha}\eta(t)$ denote the α-order Caputo derivative and the α-order integral for a function $\eta(t)$, respectively. $\Gamma(\cdot)$ denotes the gamma function. sign$(\cdot)$ is the signum function. $E_{\phi q}(t)$ and $E_{\phi}(t)$ denote the double-parameter and single-parameter Mittag–Leffler functions, respectively.

2. Fundamental Knowledge and Network Models

This section introduces the relevant definitions, assumptions, and lemmas. Then, we give fractional-order drive-response NNs that include multiple uncertainties and fuzzy operators.

Definition 1 ([31]). *The α-order Caputo derivative of $\eta(t)$ is*

$$ {}_{t_0}^{c}\mathscr{D}_t^{\alpha}\eta(t) = \frac{1}{\Gamma(1-\alpha)}\int_{t_0}^{t}(t-\omega)^{-\alpha}\eta'(\omega)d\omega,\ t \geq t_0, \tag{1}$$

where $0 < \alpha < 1$, and $\Gamma(\cdot)$ denotes the gamma function.

Definition 2 ([31]). *The α-order integral of $\eta(t)$ is*

$$ {}_{t_0}I_t^{\alpha}\eta(t) = \frac{1}{\Gamma(\alpha)}\int_{t_0}^{t}(t-\omega)^{\alpha-1}\eta(\omega)d\omega,\ t \geq t_0, \tag{2}$$

where $\alpha > 0$.

Consider nonlinear UFODCNNs with two types of fuzzy operators as below:

$$\begin{cases} {}_{t_0}^{c}\mathscr{D}_t^{\alpha}\varrho_m(t) = -(b_m + \Delta b_m(t))\varrho_m(t) + \sum\limits_{n=1}^{k}(c_{mn} + \Delta c_{mn}(t))h_n(\varrho_n(t)) \\ \qquad\qquad + \sum\limits_{n=1}^{k} a_{mn}x_n + \bigwedge\limits_{n=1}^{k} u_{mn}g_n(\varrho_n(t-\tau)) + \bigvee\limits_{n=1}^{k} v_{mn}g_n(\varrho_n(t-\tau)) \\ \qquad\qquad + \bigwedge\limits_{n=1}^{k} \widehat{P}_{mn}x_n + \bigvee\limits_{n=1}^{k} \widehat{Q}_{mn}x_n + I_m, \\ \varrho_m(t) = \beta_m(t), t \in [-\tau, t_0], \end{cases} \tag{3}$$

where $0 < \alpha < 1$, and $m \in \mathbb{N}_1^k$. $\varrho_m(t)$ represents the m-th neuron state. $h_n(\cdot)$ and $g_n(\cdot)$ represent the activation functions of the n-th neuron. $\tau > 0$ signifies the constant delay. b_m denotes the self-regulating coefficient. $\Delta b_m(t)$ and $\Delta c_{mn}(t)$ are the bounded uncertainties satisfying the constraints $|\Delta b_m(t)| \leq \Xi_m$ and $|\Delta c_{mn}(t)| \leq \Pi_{mn}$. x_m and I_m represent the input and bias. $\bigwedge$ and $\bigvee$ signify the fuzzy operators AND and OR. c_{mn} and a_{mn} characterize elements of feedback and feed-forward templates. u_{mn} and v_{mn} signify elements of feedback MIN and MAX templates. $\widehat{P}_{mn}$ and $\widehat{Q}_{mn}$ signify feed-forward MIN and MAX templates.

Take fractional-order NNs (3) as the drive system, and one can get the response system as

$$\begin{cases} {}_{t_0}^{c}\mathscr{D}_t^{\alpha}\rho_m(t) = -(b_m + \Delta b_m(t))\rho_m(t) + \sum\limits_{n=1}^{k}(c_{mn} + \Delta c_{mn}(t))h_n(\rho_n(t)) \\ \qquad\qquad + \sum\limits_{n=1}^{k} a_{mn}x_n + \bigwedge\limits_{n=1}^{k} u_{mn}g_n(\rho_n(t-\tau)) + \bigvee\limits_{n=1}^{k} v_{mn}g_n(\rho_n(t-\tau)) \\ \qquad\qquad + \bigwedge\limits_{n=1}^{k} \widehat{P}_{mn}x_n + \bigvee\limits_{n=1}^{k} \widehat{Q}_{mn}x_n + I_m + \Theta_m(t), \\ \rho_m(t) = \gamma_m(t), t \in [-\tau, t_0], \end{cases} \tag{4}$$

where $0 < \alpha < 1$, and $m \in \mathbb{N}_1^k$. $\rho_m(t)$ represents the m-th response neuron state. $\Theta_m(t)$ signifies the feedback controller with appropriate adaptive laws. $\gamma_m(t)$ is the initial value of system (4). The meanings of the remaining parameters can be inferred from the fractional-order NNs (3).

We define the m-th neuron error as $\epsilon_m(t) = \rho_m(t) - \varrho_m(t)$. Based on drive-response NNs (3) and (4), one can deduce that the error variable satisfies

$$\begin{cases} {}_{t_0}^{c}\mathscr{D}_t^{\alpha}\epsilon_m(t) = -(b_m + \Delta b_m(t))\epsilon_m(t) + \sum\limits_{n=1}^{k}(c_{mn} + \Delta c_{mn}(t))\Big[h_n(\rho_n(t)) - h_n(\varrho_n(t))\Big] \\ \qquad\qquad + \bigwedge\limits_{n=1}^{k} u_{mn}g_n(\rho_n(t-\tau)) - \bigwedge\limits_{n=1}^{k} u_{mn}g_n(\varrho_n(t-\tau)) \\ \qquad\qquad + \bigvee\limits_{n=1}^{k} v_{mn}g_n(\rho_n(t-\tau)) - \bigvee\limits_{n=1}^{k} v_{mn}g_n(\varrho_n(t-\tau)) + \Theta_m(t) \\ \epsilon_m(t) = \varphi_m(t), t \in [-\tau, t_0], \end{cases} \tag{5}$$

where $0 < \alpha < 1$, and $m \in \mathbb{N}_1^k$.

Remark 1. *Integer-order calculus has been widely used in network system modeling and various synchronous behavior research, such as the bipartite synchronization [26], the asymptotic synchronization [27], the complete synchronization [28], and the master–slave synchronization [29]. However, these feedback control or adaptive control schemes cannot be directly utilized for fractional-order NNs because of the significant difference in properties between the two types of calculus.*

Remark 2. *The FT synchronization of fractional-order NNs has attracted the attention of scholars. Refs. [38,40] considered the FT Mittag–Leffler synchronization of fractional NNs, but they ignored fuzzy characteristics and uncertainties. Refs. [34,41] studied the FT synchronization of fractional fuzzy NNs, but the model did not consider uncertainties. This article considers both uncertainties and fuzziness in the network model and simultaneously studies the FT synchronization and FT Mittag–Leffler synchronization of the network. Accordingly, the model and synchronization type in this article are more generalized than those in the literature mentioned above.*

Definition 3 ([31]). *A double-parameter Mittag–Leffler function can be defined by*

$$E_{\alpha q}(t) = \sum_{\mu=0}^{\infty} \frac{t^{\mu}}{\Gamma(\mu\alpha + q)}, \tag{6}$$

where $\alpha, q > 0$. For $q = 1$, the simplified single-parameter version is given by

$$E_{\alpha}(t) = \sum_{\mu=0}^{\infty} \frac{t^{\mu}}{\Gamma(\mu\alpha + 1)}. \tag{7}$$

Definition 4 ([41]). *For $\|\varphi\| = sup_{s\in[-\tau,t_0]}\|\varphi(s)\|$, UFODCNNs (3) and (4) are FT synchronized with respect to $\{\sigma, \varepsilon, \underline{t}, \bar{t}\}$ if $\|\varphi\| \leq \sigma$ signifies $\|\epsilon(t)\| \leq \varepsilon$ for $t \in [\underline{t}, \bar{t}]$, where $0 < \sigma < \varepsilon$.*

Definition 5 ([40]). *UFODCNNs (3) and (4) are FT Mittag–Leffler synchronized with respect to $\{\sigma, \varepsilon, \underline{t}, \bar{t}\}$ if $\|\varphi\| \leq \sigma$ signifies $\|\epsilon(t)\| \leq \iota(\sigma)E_{\alpha}(-\phi(t - t_0)^{\alpha}) \leq \varepsilon$ for $t \in [\underline{t}, \bar{t}]$, where $t_0 < \underline{t} < \bar{t}$, $0 < \sigma < \varepsilon, \phi > 0, 0 < \alpha < 1$, and $\iota(\sigma)$ denotes a nonnegative function.*

Remark 3. *Currently, there exist two types of FT synchronization. The first one is where the synchronization error of the system tends to zero in a finite time. The second is where the synchronization error is not above the desired threshold during the transients. In this article, we mainly focus on the second type (Definitions 4 and 5).*

Lemma 1 ([32]). *For a function $\Phi(t) \in \mathbb{C}^1([t_0, +\infty), \mathbb{R})$, we obtain*

$$^{c}_{t_0}\mathscr{D}^{\alpha}_{t}|\Phi(t)| \leq sign(\Phi(t))\,^{c}_{t_0}\mathscr{D}^{\alpha}_{t}\Phi(t),\ 0 < \alpha < 1. \tag{8}$$

Assumption 1 ([51]). *For $\forall \vartheta_1, \vartheta_2 \in \mathbb{R}$, there exist constants $\mathcal{L}^h_n > 0$ and $\mathcal{L}^g_n > 0$ satisfying*

$$|h_n(\vartheta_2) - h_n(\vartheta_1)| \leq \mathcal{L}^h_n|\vartheta_2 - \vartheta_1|, \tag{9}$$

and

$$|g_n(\vartheta_2) - g_n(\vartheta_1)| \leq \mathcal{L}^g_n|\vartheta_2 - \vartheta_1|, \tag{10}$$

where $n \in \mathbb{N}^k_1$.

Lemma 2 ([15]). *If ρ_n and ϱ_n signify different states of UFODCNNs (3) and (4), then we can obtain*

$$\Big|\bigwedge_{n=1}^{k} u_{mn}g_n(\rho_n(t-\tau)) - \bigwedge_{n=1}^{k} u_{mn}g_n(\varrho_n(t-\tau))\Big| \leq \sum_{n=1}^{k} |u_{mn}||g_n(\rho_n(t-\tau)) - g_n(\varrho_n(t-\tau))|, \tag{11}$$

and

$$\Big|\bigvee_{n=1}^{k} v_{mn}g_n(\rho_n(t-\tau)) - \bigvee_{n=1}^{k} v_{mn}g_n(\varrho_n(t-\tau))\Big| \leq \sum_{n=1}^{k} |v_{mn}||g_n(\rho_n(t-\tau)) - g_n(\varrho_n(t-\tau))|, \tag{12}$$

where $m, n \in \mathbb{N}^k_1$.

Lemma 3 ([41]). *Let $0 < \alpha < 1, \phi > 0, \psi \leq 0$, and $W_1(t)$ and $W_2(t)$ be nonnegative functions satisfying*

$$ {}_{t_0}^{c}\mathscr{D}_t^{\alpha}(W_1(t) + W_2(t)) \leq -\phi W_1(t) + \psi, \ t \geq t_0. \tag{13}$$

Then, for $\forall \lambda > 0$, there is a constant $\bar{t}$ such that

$$W_1(t) \leq \left(W_1(t_0) + W_2(t_0) + \lambda - \frac{\psi}{\phi}\right) E_{\alpha}(-\phi(t - t_0)^{\alpha}) + \frac{\psi}{\phi}, \tag{14}$$

where $t \in [t_0, \bar{t}]$, and $\bar{t}$ signifies the solution of $E_{\alpha}(-\phi(t - t_0)^{\alpha}) - \frac{W_1(t_0)+W_2(t_0)}{W_1(t_0)+W_2(t_0)+\lambda} = 0$.

3. New Synchronization Results of UFODCNNs

To accomplish the FT synchronization mission between UFODCNNs (3) and (4), we consider an information feedback controller with adaptive laws as follows:

$$\Theta_m(t) = \begin{cases} -\chi \frac{\epsilon_m(t)}{|\epsilon_m(t)|}|\epsilon_m(t - \tau)| - \varsigma_m(t)\epsilon_m(t) - \delta \frac{\epsilon_m(t)}{|\epsilon_m(t)|}, \ |\epsilon_m(t)| \neq 0, \\ 0, \ |\epsilon_m(t)| = 0, \end{cases} \tag{15}$$

where $\varsigma_m(t)$ represents the variable feedback strength satisfying ${}_{t_0}^{c}\mathscr{D}_t^{\alpha}\varsigma_m(t) = \kappa_m|\epsilon_m(t)|$, $m \in \mathbb{N}_1^k$. χ, δ, and κ_m signify positive control parameters.

Remark 4. *Figure 1 shows the control block diagram between drive system (3) and response system (4). When the error norm does not conform to the synchronization definition, the nonlinear adaptive controller (15) composed of three stacked submodules is applied to the response system. The systems stop external control input when the synchronization goal is achieved.*

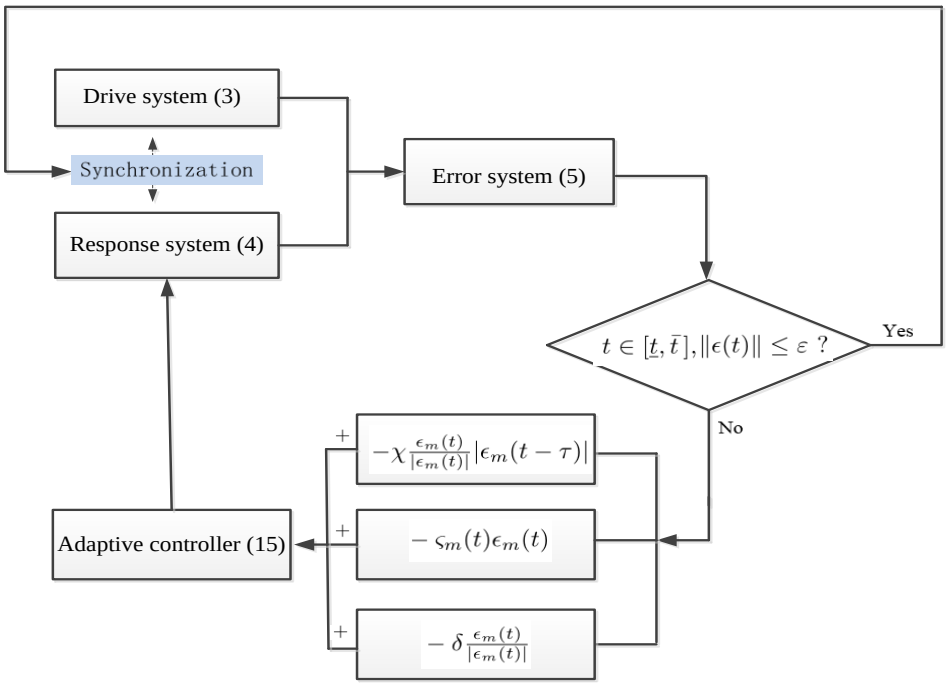

Figure 1. The control block diagram between drive system (3) and response system (4).

Remark 5. *Different from the nonadaptive feedback control schemes in [16,50–52], this article devises an adaptive nonlinear feedback controller including two situations, i.e.,* $\epsilon_m(t) = 0$ *and* $\epsilon_m(t) \neq 0$*. The information feedback with three feedback modules is activated only under the situation* $\epsilon_m(t) \neq 0$*. Particularly, the first module* $-\chi \frac{\epsilon_m(t)}{|\epsilon_m(t)|}|\epsilon_m(t-\tau)|$ *can deal with the impact of delays on system stability. The second module* $-\varsigma_m(t)\epsilon_m(t)$ *can adaptively remove quasi-linear growth errors. The adaptive law reflects that the feedback strength automatically adjusts its size as the error changes. The rest module* $-\delta \frac{\epsilon_m(t)}{|\epsilon_m(t)|}$ *has the function of reducing the synchronization error between the drive–response NNs. These three functional modules have distinct functions and are indispensable for handling network synchronization problems that involve uncertainties and delays.*

Remark 6. *Various conventional PID controllers [17,18] and improved versions [19–21] have demonstrated excellent performance in handling integer-order linear and nonlinear systems. Compared to these PID controllers, our adaptive nonlinear controller is designed for the specific structure of fractional-order UFODCNNs with fuzzy operators. First, the network model in this article is a fractional-order nonlinear delayed system. Our controller features a dedicated time-delayed feedback module that enables direct compensation of the system's time-delayed state. In contrast, the neuroendocrine PID controller [20] and the BELBIC PID controller [21] focus on set-point regulation or non-delayed systems, lacking direct compensation mechanisms for historical states (time-delayed states). Second, the network model in this article has uncertain factors caused by parameter uncertainties and fuzzy rules. Our controller includes an adaptive feedback module, and the feedback strength is adaptively adjusted by the real-time system error, which can better address the impact of uncertain factors on the system's stability. However, the feedback gains of the conventional PID controller [17,18] and the Sigmoid PID controller [19] are often predefined and do not have a real-time adaptive processing mechanism for uncertain information.*

3.1. FT Synchronization Criteria

Theorem 1. *Under Assumption 1 and adaptive feedback controller (15), UFODCNNs (3) are FT synchronized with UFODCNNs (4) with respect to* $\{\sigma, \varepsilon, \underline{t}, \bar{t}\}$ *if*

$$\Big(\sigma + W_2(t_0) + \lambda - \frac{\psi}{\phi}\Big) E_\alpha\Big(-\phi(t-t_0)^\alpha\Big) + \frac{\psi}{\phi} \leq \varepsilon,\ t \in [\underline{t}, \bar{t}\,], \tag{16}$$

$$\varsigma^* > max_{1\leq m\leq k}\left[-b_m + \Xi_m + \sum_{n=1}^{k}\Big(|c_{nm}| + \Pi_{nm}\Big)\mathcal{L}_m^h\right], \tag{17}$$

$$\chi > max_{1\leq m\leq k}\left[\sum_{n=1}^{k}\Big(|u_{nm}| + |v_{nm}|\Big)\mathcal{L}_m^g\right], \tag{18}$$

where $\phi = min_{1\leq m\leq k}\left[b_m - \Xi_m - \sum\limits_{n=1}^{k}\Big(|c_{nm}| + \Pi_{nm}\Big)\mathcal{L}_m^h + \varsigma^*\right] > 0$ *and* $\psi = -k\delta$*.* $\bar{t}$ *and* $\underline{t}$ *denote the solutions of* $E_\alpha\Big(-\phi(t-t_0)^\alpha\Big) - \frac{W_1(t_0)+W_2(t_0)}{W_1(t_0)+W_2(t_0)+\lambda} = 0$ *and* $E_\alpha\Big(-\phi(t-t_0)^\alpha\Big) - \frac{\varepsilon-\frac{\psi}{\phi}}{\sigma+W_2(t_0)+\lambda-\frac{\psi}{\phi}} = 0$*, respectively.* $W_1(t_0) = \sum\limits_{m=1}^{k}|\epsilon_m(t_0)|$ *and* $W_2(t_0) = \sum\limits_{m=1}^{k}\frac{(\varsigma_m(t_0)-\varsigma^*)^2}{2\kappa_m}$*.*

Proof. Consider an auxiliary function

$$W(t) = \overbrace{\sum_{m=1}^{k} |\epsilon_m(t)|}^{W_1(t)} + \overbrace{\sum_{m=1}^{k} \frac{(\varsigma_m(t)-\varsigma^*)^2}{2\kappa_m}}^{W_2(t)}. \tag{19}$$

Based on Lemma 1, computing the α-order derivative of $W(t)$ gives

$$\begin{aligned}
&{}_{t_0}^{c}\mathscr{D}_t^{\alpha} W(t) \\
&=_{t_0}^{c} \mathscr{D}_t^{\alpha}\left[\textstyle\sum_{m=1}^{k} |\epsilon_m(t)| + \sum_{m=1}^{k} \frac{(\varsigma_m(t)-\varsigma^*)^2}{2\kappa_m}\right] \\
&\le \textstyle\sum_{m=1}^{k} \operatorname{sign}(\epsilon_m(t)) {}_{t_0}^{c}\mathscr{D}_t^{\alpha}\epsilon_m(t) + \sum_{m=1}^{k} \frac{\varsigma_m(t)-\varsigma^*}{\kappa_m} {}_{t_0}^{c}\mathscr{D}_t^{\alpha}\varsigma_m(t) \\
&= \textstyle\sum_{m=1}^{k} \operatorname{sign}(\epsilon_m(t))\Big\{ -(b_m + \Delta b_m(t))\epsilon_m(t) + \sum_{n=1}^{k} (c_{mn} + \Delta c_{mn}(t))\Big[h_n(\rho_n(t)) - h_n(\varrho_n(t))\Big] \\
&\quad + \bigwedge_{n=1}^{k} u_{mn} g_n(\rho_n(t-\tau)) - \bigwedge_{n=1}^{k} u_{mn} g_n(\varrho_n(t-\tau)) + \bigvee_{n=1}^{k} v_{mn} g_n(\rho_n(t-\tau)) \\
&\quad - \bigvee_{n=1}^{k} v_{mn} g_n(\varrho_n(t-\tau)) - \chi \tfrac{\epsilon_m(t)|\epsilon_m(t-\tau)|}{|\epsilon_m(t)|} - \varsigma_m(t)\epsilon_m(t) - \delta \tfrac{\epsilon_m(t)}{|\epsilon_m(t)|} \Big\} \\
&\quad + \textstyle\sum_{m=1}^{k} (\varsigma_m(t) - \varsigma^*)|\epsilon_m(t)|.
\end{aligned} \tag{20}$$

Considering the boundedness of uncertainties and the Lipschitz condition of the function $h(\cdot)$, one can get

$$\sum_{m=1}^{k} \operatorname{sign}(\epsilon_m(t))\Big[-(b_m + \Delta b_m(t))\Big]\epsilon_m(t) \le \sum_{m=1}^{k} (-b_m + \Xi_m)|\epsilon_m(t)|, \tag{21}$$

and

$$\begin{aligned}
&\sum_{m=1}^{k} \operatorname{sign}(\epsilon_m(t)) \sum_{n=1}^{k} (c_{mn} + \Delta c_{mn}(t))\Big[h_n(\rho_n(t)) - h_n(\varrho_n(t))\Big] \\
&\quad \le \sum_{m=1}^{k}\sum_{n=1}^{k} (|c_{mn}| + \Pi_{mn})|h_n(\rho_n(t)) - h_n(\varrho_n(t))| \\
&\quad \le \sum_{m=1}^{k}\sum_{n=1}^{k} (|c_{mn}| + \Pi_{mn})\mathcal{L}_n^h|\epsilon_n(t)|.
\end{aligned} \tag{22}$$

Based on Lemma 2 and Assumption 1, one can obtain

$$\begin{aligned}
&\sum_{m=1}^{k} \operatorname{sign}(\epsilon_m(t))\Big[\bigwedge_{n=1}^{k} u_{mn} g_n(\rho_n(t-\tau)) - \bigwedge_{n=1}^{k} u_{mn} g_n(\varrho_n(t-\tau))\Big] \\
&\quad \le \sum_{m=1}^{k}\sum_{n=1}^{k} |u_{mn}||g_n(\rho_n(t-\tau)) - g_n(\varrho_n(t-\tau))| \\
&\quad \le \sum_{m=1}^{k}\sum_{n=1}^{k} |u_{mn}|\mathcal{L}_n^g|\epsilon_n(t-\tau)|,
\end{aligned} \tag{23}$$

and

$$\begin{aligned}
&\sum_{m=1}^{k} \operatorname{sign}(\epsilon_m(t))\Big[\bigvee_{n=1}^{k} v_{mn}g_n(\rho_n(t-\tau)) - \bigvee_{n=1}^{k} v_{mn}g_n(\varrho_n(t-\tau))\Big] \\
&\quad \le \sum_{m=1}^{k}\sum_{n=1}^{k} |v_{mn}||g_n(\rho_n(t-\tau)) - g_n(\varrho_n(t-\tau))| \\
&\quad \le \sum_{m=1}^{k}\sum_{n=1}^{k} |v_{mn}|\mathcal{L}_n^g|\epsilon_n(t-\tau)|.
\end{aligned} \tag{24}$$

Substituting inequalities (21)–(24) into (20), one derives

$$\begin{aligned}
&{}_{t_0}^{c}\mathscr{D}_t^{\alpha} W(t) \\
&\le \sum_{m=1}^{k}\Bigg[(-b_m+\Xi_m)|\epsilon_m(t)| + \sum_{n=1}^{k}(|c_{mn}|+\Pi_{mn})\mathcal{L}_n^h|\epsilon_n(t)| + \sum_{n=1}^{k}|u_{mn}|\mathcal{L}_n^g|\epsilon_n(t-\tau)| \\
&\quad + \sum_{n=1}^{k}|v_{mn}|\mathcal{L}_n^g|\epsilon_n(t-\tau)| - \chi|\epsilon_m(t-\tau)| - \varsigma_m(t)|\epsilon_m(t)| - \delta\Bigg] + \sum_{m=1}^{k}(\varsigma_m(t)-\varsigma^*)|\epsilon_m(t)| \\
&\le \sum_{m=1}^{k}\Bigg[-b_m+\Xi_m+\sum_{n=1}^{k}(|c_{nm}|+\Pi_{nm})\mathcal{L}_m^h - \varsigma^*\Bigg]|\epsilon_m(t)| \\
&\quad + \sum_{m=1}^{k}\Bigg[-\chi+\sum_{n=1}^{k}(|u_{nm}|+|v_{nm}|)\mathcal{L}_m^g\Bigg]|\epsilon_m(t-\tau)| - \sum_{m=1}^{k}\delta.
\end{aligned} \tag{25}$$

Let $\phi = \min_{1\le m\le k}\Big[b_m - \Xi_m - \sum_{n=1}^{k}\Big(|c_{nm}|+\Pi_{nm}\Big)\mathcal{L}_m^h + \varsigma^*\Big] > 0$ and $\psi = -k\delta$. Then, one can get

$${}_{t_0}^{c}\mathscr{D}_t^{\alpha}(W_1(t)+W_2(t)) \le -\phi W_1(t) + \psi. \tag{26}$$

By Lemma 3, for $\forall\lambda > 0$, there exists an instant $\bar{t}$ such that

$$\|\epsilon(t)\| = W_1(t) \le \Big(W_1(t_0)+W_2(t_0)+\lambda-\frac{\psi}{\phi}\Big)E_{\alpha}\Big(-\phi(t-t_0)^{\alpha}\Big) + \frac{\psi}{\phi}, \tag{27}$$

where $t \in [t_0, \bar{t}\,]$, and $\bar{t}$ denotes the solution of $E_{\alpha}\Big(-\phi(t-t_0)^{\alpha}\Big) - \frac{W_1(t_0)+W_2(t_0)}{W_1(t_0)+W_2(t_0)+\lambda} = 0$.

According to Definition 4 and condition (16), one can obtain

$$\|\epsilon(t)\| \le \Big(\sigma+W_2(t_0)+\lambda-\frac{\psi}{\phi}\Big)E_{\alpha}\Big(-\phi(t-t_0)^{\alpha}\Big) + \frac{\psi}{\phi} \le \varepsilon, \tag{28}$$

where $t \in [\underline{t}, \bar{t}\,]$, and $\underline{t}$ is the solution of $E_{\alpha}\Big(-\phi(t-t_0)^{\alpha}\Big) - \frac{\varepsilon-\frac{\psi}{\phi}}{\sigma+W_2(t_0)+\lambda-\frac{\psi}{\phi}} = 0$. □

Remark 7. *Combining the relevant mathematical formulas, lemmas, and assumptions, Figure 2 shows a schematic diagram of the proof of Theorem 1. It describes the logical derivation relationship of the mathematical expressions (16)–(28). The proof idea is to first construct a positive auxiliary function (19) based on stability theory and solve for the fractional derivative of the function to obtain (20). Using the Lipschitz condition, one can obtain inequalities (21) and (22) and obtain inequalities (23) and (24) based on Lemma 2 and Assumption 1. Then, we substitute (21)–(24) into (20) for simplification and use conditions (16)–(18) and Definition 4 to obtain inequalities (26)–(28).*

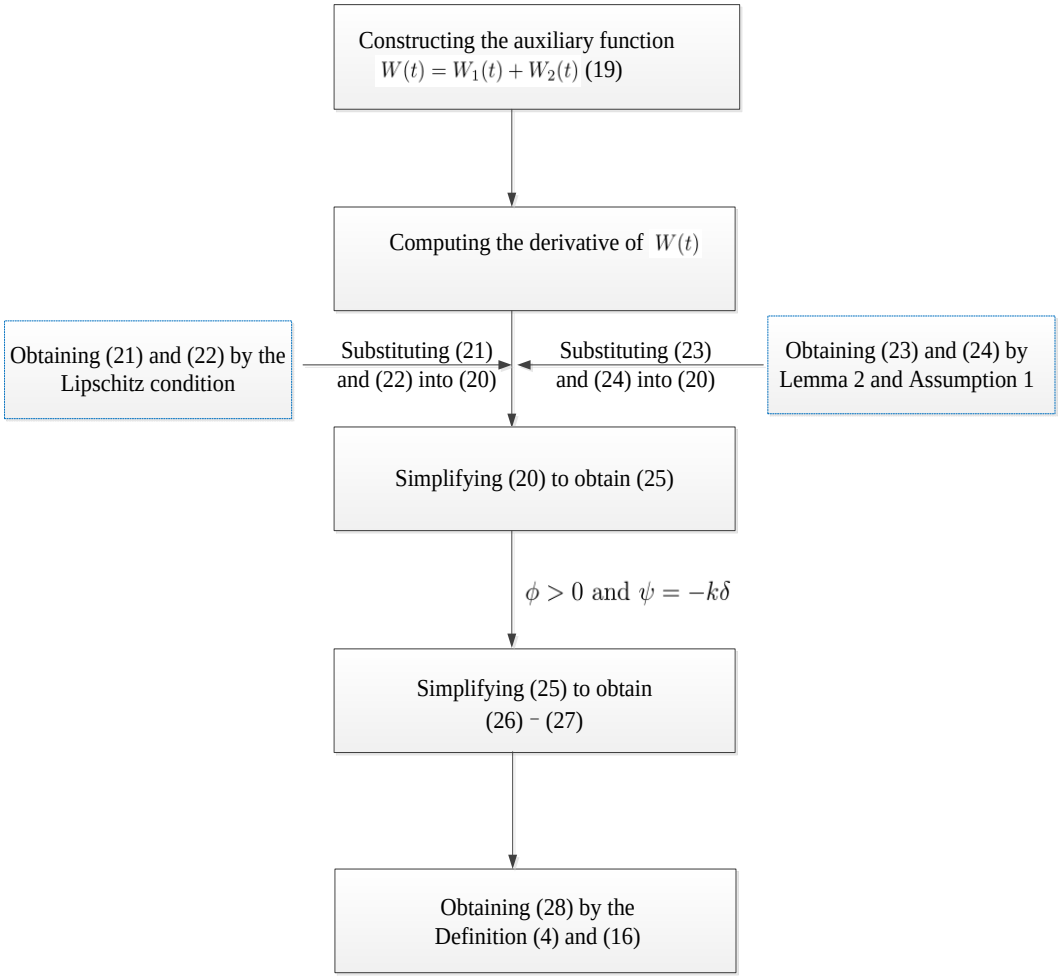

Figure 2. The schematic derivation of the proof process for Theorem 1.

In view of $\phi > 0$ and $\psi \leq 0$, we get $\frac{\psi}{\phi} \leq 0$. Based on the proof of Theorem 1, one can obtain the following FT Mittag–Leffler synchronization results.

3.2. FT Mittag–Leffler Synchronization Criteria

Theorem 2. *Under Assumption 1 and adaptive feedback controller (15), UFODCNNs (3) are FT Mittag–Leffler synchronized with UFODCNNs (4) with respect to* $\{\sigma, \varepsilon, \underline{t}, \bar{t}\}$ *if*

$$\Big(\sigma + W_2(t_0) + \lambda - \frac{\psi}{\phi}\Big) E_\alpha\Big(-\phi(t-t_0)^\alpha\Big) \leq \varepsilon,\ t \in [\underline{t}, \bar{t}], \tag{29}$$

$$\varsigma^* > max_{1\leq m\leq k}\left[-b_m + \Xi_m + \sum_{n=1}^{k}\Big(|c_{nm}| + \Pi_{nm}\Big)\mathcal{L}_m^h\right], \tag{30}$$

$$\chi > max_{1\leq m\leq k}\left[\sum_{n=1}^{k}\Big(|u_{nm}| + |v_{nm}|\Big)\mathcal{L}_m^g\right], \tag{31}$$

where $\phi = min_{1\le m\le k}\left[b_m - \Xi_m - \sum\limits_{n=1}^{k}\Big(|c_{nm}| + \Pi_{nm}\Big)\mathcal{L}_m^h + \varsigma^*\right] > 0$, *and* $\psi = -k\delta$. $\bar{t}$ *and* $\underline{t}$ *denote the solutions of* $E_\alpha\Big(-\phi(t-t_0)^\alpha\Big) - \frac{W_1(t_0)+W_2(t_0)}{W_1(t_0)+W_2(t_0)+\lambda} = 0$ *and* $E_\alpha\Big(-\phi(t-t_0)^\alpha\Big) - \frac{\varepsilon}{\sigma+W_2(t_0)+\lambda-\frac{\psi}{\phi}} = 0$, *respectively.* $W_1(t_0) = \sum\limits_{m=1}^{k}|\epsilon_m(t_0)|$, *and* $W_2(t_0) = \sum\limits_{m=1}^{k}\frac{(\varsigma_m(t_0)-\varsigma^*)^2}{2\kappa_m}$.

Proof. Using the similar proof steps with Theorem 1, for $\forall\lambda > 0$, there exists an instant $\bar{t}$ such that

$$\|\epsilon(t)\| = W_1(t) \le \Big(W_1(t_0) + W_2(t_0) + \lambda - \frac{\psi}{\phi}\Big)E_\alpha\Big(-\phi(t-t_0)^\alpha\Big) + \frac{\psi}{\phi}, \tag{32}$$

where $t \in [t_0, \bar{t}\,]$, and $\bar{t}$ denotes the solution of $E_\alpha\Big(-\phi(t-t_0)^\alpha\Big) - \frac{W_1(t_0)+W_2(t_0)}{W_1(t_0)+W_2(t_0)+\lambda} = 0$.

According to Definition 5 and condition (29) as well as $\frac{\psi}{\phi} \le 0$, one can get

$$\|\epsilon(t)\| \le \Big(\sigma + W_2(t_0) + \lambda - \frac{\psi}{\phi}\Big)E_\alpha\Big(-\phi(t-t_0)^\alpha\Big) \le \varepsilon, \tag{33}$$

where $t \in [\underline{t}, \bar{t}\,]$, and $\underline{t}$ is the solution of $E_\alpha\Big(-\phi(t-t_0)^\alpha\Big) - \frac{\varepsilon}{\sigma+W_2(t_0)+\lambda-\frac{\psi}{\phi}} = 0$. □

3.3. FT Synchronization Corollary

If uncertainties are not taken into account, then fractional-order NNs (3) and (4) are simplified by

$$\begin{cases} {}_{t_0}^{c}\mathscr{D}_t^\alpha \varrho_m(t) = -b_m\varrho_m(t) + \sum\limits_{n=1}^{k} c_{mn}h_n(\varrho_n(t)) + \sum\limits_{n=1}^{k} a_{mn}x_n \\ \qquad\qquad + \bigwedge\limits_{n=1}^{k} u_{mn}g_n(\varrho_n(t-\tau)) + \bigvee\limits_{n=1}^{k} v_{mn}g_n(\varrho_n(t-\tau)) \\ \qquad\qquad + \bigwedge\limits_{n=1}^{k} \widehat{P}_{mn}x_n + \bigvee\limits_{n=1}^{k} \widehat{Q}_{mn}x_n + I_m, \\ \varrho_m(t) = \beta_m(t), t \in [-\tau, t_0], \end{cases} \tag{34}$$

and

$$\begin{cases} {}_{t_0}^{c}\mathscr{D}_t^\alpha \rho_m(t) = -b_m\rho_m(t) + \sum\limits_{n=1}^{k} c_{mn}h_n(\rho_n(t)) + \sum\limits_{n=1}^{k} a_{mn}x_n \\ \qquad\qquad + \bigwedge\limits_{n=1}^{k} u_{mn}g_n(\rho_n(t-\tau)) + \bigvee\limits_{n=1}^{k} v_{mn}g_n(\rho_n(t-\tau)) \\ \qquad\qquad + \bigwedge\limits_{n=1}^{k} \widehat{P}_{mn}x_n + \bigvee\limits_{n=1}^{k} \widehat{Q}_{mn}x_n + I_m + \Theta_m(t), \\ \rho_m(t) = \gamma_m(t), t \in [-\tau, t_0], \end{cases} \tag{35}$$

where $0 < \alpha < 1$, and $m \in \mathbb{N}_1^k$. By the adaptive feedback controller (15), we obtain the following corollary utilizing a similar proof to that of Theorem 1.

Corollary 1. *Under Assumption 1 and adaptive feedback controller (15), UFODCNNs (34) are FT synchronized with UFODCNNs (35) with respect to* $\{\sigma, \varepsilon, \underline{t}, \bar{t}\,\}$ *if*

$$\Big(\sigma + W_2(t_0) + \lambda - \frac{\psi}{\phi}\Big)E_\alpha\Big(-\phi(t-t_0)^\alpha\Big) + \frac{\psi}{\phi} \le \varepsilon,\ t \in [\underline{t}, \bar{t}\,], \tag{36}$$

$$\varsigma^* > max_{1\le m\le k}\left[-b_m + \sum_{n=1}^{k}|c_{nm}|\mathcal{L}_m^h\right], \tag{37}$$

$$\chi > max_{1\le m\le k}\left[\sum_{n=1}^{k}\Big(|u_{nm}| + |v_{nm}|\Big)\mathcal{L}_m^g\right], \tag{38}$$

where $\phi = min_{1\le m\le k}\left[b_m - \sum\limits_{n=1}^{k}|c_{nm}|\mathcal{L}_m^h + \varsigma^*\right] > 0$, *and* $\psi = -k\delta$. $\bar{t}$ *and* $\underline{t}$ *denote the solutions of* $E_\alpha\Big(-\phi(t-t_0)^\alpha\Big) - \frac{W_1(t_0)+W_2(t_0)}{W_1(t_0)+W_2(t_0)+\lambda} = 0$ *and* $E_\alpha\Big(-\phi(t-t_0)^\alpha\Big) - \frac{\varepsilon-\frac{\psi}{\phi}}{\sigma+W_2(t_0)+\lambda-\frac{\psi}{\phi}} = 0$, *respectively.* $W_1(t_0) = \sum\limits_{m=1}^{k}|\epsilon_m(t_0)|$, *and* $W_2(t_0) = \sum\limits_{m=1}^{k}\frac{(\varsigma_m(t_0)-\varsigma^*)^2}{2\kappa_m}$.

Proof. The overall proof approach and steps are the same as Theorem 1; so, we omit them here. □

Remark 8. *According to (34) and (35) and Corollary 1, if we replace* $\Big(\sigma + W_2(t_0) + \lambda - \frac{\psi}{\phi}\Big)E_\alpha\Big(-\phi(t-t_0)^\alpha\Big) + \frac{\psi}{\phi} \le \varepsilon,\ t \in [\underline{t}, \bar{t}\,]$ *with* $\Big(\sigma + W_2(t_0) + \lambda - \frac{\psi}{\phi}\Big)E_\alpha\Big(-\phi(t-t_0)^\alpha\Big) \le \varepsilon,\ t \in [\underline{t}, \bar{t}\,]$, *and replace* $E_\alpha\Big(-\phi(t-t_0)^\alpha\Big) - \frac{\varepsilon-\frac{\psi}{\phi}}{\sigma+W_2(t_0)+\lambda-\frac{\psi}{\phi}} = 0$ *with* $E_\alpha\Big(-\phi(t-t_0)^\alpha\Big) - \frac{\varepsilon}{\sigma+W_2(t_0)+\lambda-\frac{\psi}{\phi}} = 0$, *a similar FT Mittag–Leffler synchronization Corollary can be obtained,*

Remark 9. *For the FT interval* $[t_0, t_0+T]$ *in [38,40], the left end point is unchanged, and the right end point* T *is updated with* σ *and* ε. *However, for the FT interval* $[\underline{t}, \bar{t}\,]$ *in this article, the right end point is unchanged, and the left end point is updated with* σ *and* ε.

4. Simulation Examples

This section presents numerical examples to verify the applicability of our theorem results.

Example 1. *Consider two-dimensional nonlinear UFODCNNs with fuzzy operators as the master system:*

$$\begin{cases} {}_{t_0}^{c}\mathscr{D}_t^{0.8}\varrho_m(t) = -(b_m + \Delta b_m(t))\varrho_m(t) + \sum\limits_{n=1}^{2}(c_{mn} + \Delta c_{mn}(t))h_n(\varrho_n(t)) \\ \qquad\qquad + \sum\limits_{n=1}^{2}a_{mn}x_n + \bigwedge\limits_{n=1}^{2}u_{mn}g_n(\varrho_n(t-\tau)) + \bigvee\limits_{n=1}^{2}v_{mn}g_n(\varrho_n(t-\tau)) \\ \qquad\qquad + \bigwedge\limits_{n=1}^{2}\widehat{P}_{mn}x_n + \bigvee\limits_{n=1}^{2}\widehat{Q}_{mn}x_n + I_m, \\ \varrho_m(t) = \beta_m(t), t \in [-\tau, t_0], \end{cases} \tag{39}$$

where $b_1 = 0.6$, $b_2 = 0.5$, $\Delta b_1(t) = \Delta c_{1n}(t) = 0.1\sin t$, $\Delta b_2(t) = \Delta c_{2n}(t) = 0.1\cos t$, $h_n(\varrho) = g_n(\varrho) = \tanh(\varrho)$, $(c_{mn})_{2\times2} = \begin{bmatrix}-1.4 & -3.0\\ 0.9 & -1.5\end{bmatrix}$, $(a_{mn})_{2\times2} = \begin{bmatrix}0.3 & 0.4\\ 0.2 & 0.5\end{bmatrix}$, $(\widehat{P}_{mn})_{2\times2} = \begin{bmatrix}0.2 & 0.4\\ 0.4 & 0.2\end{bmatrix}$, $(\widehat{Q}_{mn})_{2\times2} = \begin{bmatrix}0.4 & 0.3\\ 0.5 & 0.2\end{bmatrix}$, $(u_{mn})_{2\times2} = \begin{bmatrix}-1.6 & -0.2\\ -0.4 & -2.6\end{bmatrix}$, $(v_{mn})_{2\times2} = \begin{bmatrix}-0.9 & -0.2\\ -0.3 & -1.6\end{bmatrix}$, $(x_n) = \begin{bmatrix}0.3\\ 0.3\end{bmatrix}$, *and* $I = \begin{bmatrix}0\\ 0\end{bmatrix}$.

According to the form of the activation functions, one can see that Assumption 1 holds for $\mathcal{L}_n^h = \mathcal{L}_n^g = 1$. According to fractional-order master system (39), one can get the following fractional-order slave system

$$\begin{cases} {}_{t_0}^{c}\mathscr{D}_t^{0.8}\rho_m(t) = -(b_m + \Delta b_m(t))\rho_m(t) + \sum\limits_{n=1}^{2}(c_{mn} + \Delta c_{mn}(t))h_n(\rho_n(t)) \\ \qquad\qquad + \sum\limits_{n=1}^{2} a_{mn}x_n + \bigwedge\limits_{n=1}^{2} u_{mn}g_n(\rho_n(t-\tau)) + \bigvee\limits_{n=1}^{2} v_{mn}g_n(\rho_n(t-\tau)) \\ \qquad\qquad + \bigwedge\limits_{n=1}^{2} \widehat{P}_{mn}x_n + \bigvee\limits_{n=1}^{2} \widehat{Q}_{mn}x_n + I_m + \Theta_m(t), \\ \rho_m(t) = \gamma_m(t), t \in [-\tau, t_0], \end{cases} \tag{40}$$

where the network parameters are the same as (39).

Let parameters $t_0 = 0$, $\tau = 0.3$, $\kappa_1 = \kappa_2 = 1, \sigma = 0.13, \delta = 0.01, \varsigma^* = 4.4$, and $\chi = 4.7$. Simple calculations indicate that $\varsigma^* > \max_{1\le m\le k}\left[-b_m + \Xi_m + \sum\limits_{n=1}^{k}\Big(|c_{nm}| + \Pi_{nm}\Big)\mathcal{L}_m^h\right] = 4.3$, $\chi > \max_{1\le m\le k}\left[\sum\limits_{n=1}^{k}\Big(|u_{nm}| + |v_{nm}|\Big)\mathcal{L}_m^g\right] = 4.6$, $\phi = \min_{1\le m\le k}\left[b_m - \Xi_m - \sum\limits_{n=1}^{k}\Big(|c_{nm}| + \Pi_{nm}\Big)\mathcal{L}_m^h + \varsigma^*\right] = 0.1$, $\psi = -0.02$, $\underline{t} = 2.155$, and $\bar{t} = 33.11$. Hence, all the inequality constraints in Theorem 1 are satisfied for the above parameters.

The time evolution of the adaptive control strength $\varsigma_m(t)$ of the nonlinear controller (15) is given in Figure 3. The system errors of different states are shown in Figure 4. The norm of the system error can be seen in Figure 5. To quantify the variation in the error norm, the time evolution of $\|\epsilon(t)\|$ between systems (39) and (40) is given in Table 1. Clearly, as the control advances, the master networks (39) and slave networks (40) can reach FT synchronization.

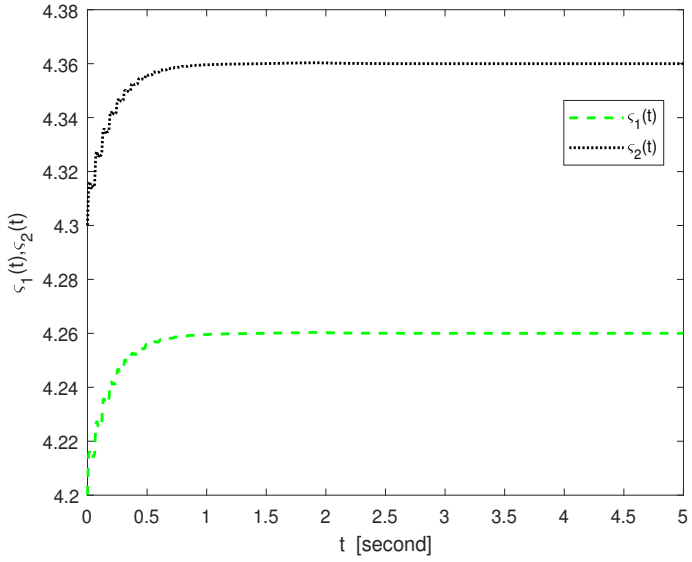

Figure 3. The time evolution of control strengths $\varsigma_m(t)$ in Example 1.

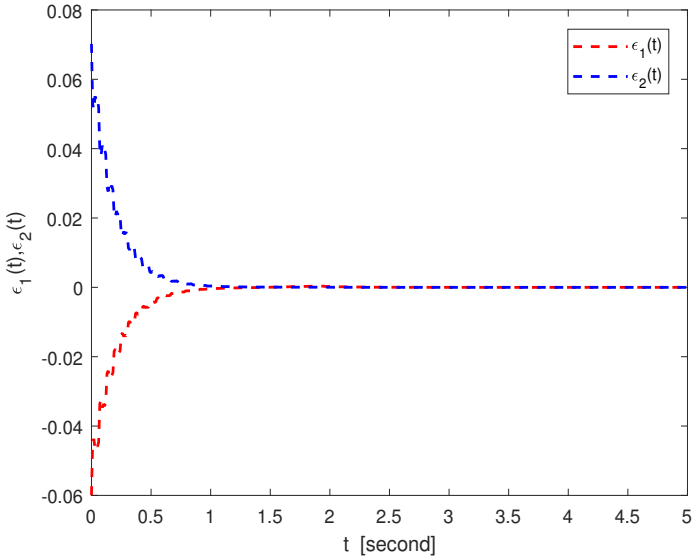

Figure 4. System errors $\epsilon_m(t)$ between fuzzy UFODCNNs (39) and (40) under adaptive controller (15) in Example 1.

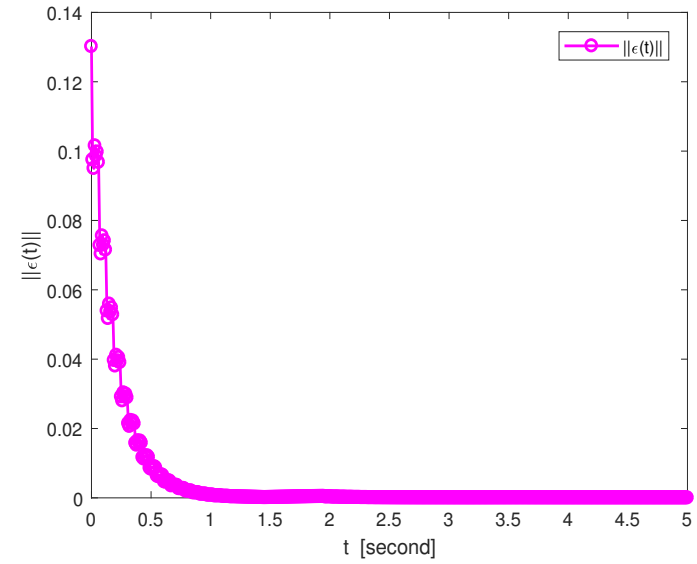

Figure 5. The norm of the system error between fuzzy UFODCNNs (39) and (40) under adaptive controller (15) in Example 1.

Table 1. The time evolution of the error norm $\|\epsilon(t)\|$ between UFODCNNs (39) and (40).

Time t	**0.1**	**0.2**	**0.4**	**0.6**	**0.8**	**1.0**	**1.2**
Error norm	0.0793	0.0418	0.0186	0.0052	0.0025	0.0010	0

To investigate the sensitivity of important parameters in this article, initial values were randomly selected $[-1, 1]$ for each experiment. First, we scanned the uncertain parameters from 0.15sint to 0.40sint with a step size of 0.05sint. Under the same conditions, we performed independent experiments on each parameter 10 times and calculated the mean and variance of the synchronization time. As shown in Table 2, the greater the uncertainty $\Delta b_1(t)$, the larger the mean time and variance for the network to reach synchronization. Second, we scanned the time delays from 0.05 to 0.5, and the results in Table 3 indicate that as the time delay increases, the network takes longer to achieve synchronization, and the

variance of the synchronization time also increases. Third, we selected different control strengths δ and χ and observed their impact on the synchronization time. As shown in Tables 4 and 5, increasing the control strengths is beneficial for reducing the synchronization time and decreasing the time variance. Regardless of how the parameters change, as long as the theorem conditions are met, the controller proposed in this paper can achieve network synchronization under small variance. This indicates that the control method proposed in this article has good robustness.

Table 2. Comparisons of mean time and variance with different uncertainties.

$\Delta b_1(t)$	0.15 sint	0.20 sint	0.25 sint	0.30 sint	0.35 sint	0.40 sint
Mean time	1.246	1.424	1.713	2.178	2.559	2.959
Variance	0.023	0.024	0.028	0.028	0.029	0.032

Table 3. Comparisons of mean time and variance with different delays.

Delays τ	0.05	0.1	0.2	0.3	0.4	0.5
Mean time	0.236	0.616	0.827	1.153	1.962	3.248
Variance	0.012	0.013	0.014	0.022	0.026	0.031

Table 4. Comparisons of mean time and variance with different strengths δ.

Strengths δ	0.01	0.02	0.03	0.04	0.05	0.06
Mean time	1.152	0.993	0.784	0.635	0.493	0.346
Variance	0.021	0.019	0.018	0.018	0.017	0.016

Table 5. Comparisons of mean time and variance with different strengths χ.

Strengths χ	4.8	4.9	5.0	5.1	5.2	5.3
Mean time	1.143	1.092	1.014	0.957	0.865	0.732
Variance	0.020	0.019	0.019	0.018	0.018	0.017

Example 2. *Consider the following two-dimensional nonlinear UFODCNNs with fuzzy operators as the master system:*

$$\begin{cases} {}_{t_0}^{c}\mathscr{D}_t^{0.92}\varrho_m(t) = -(b_m + \Delta b_m(t))\varrho_m(t) + \sum\limits_{n=1}^{2}(c_{mn} + \Delta c_{mn}(t))h_n(\varrho_n(t)) \\ \qquad\qquad + \sum\limits_{n=1}^{2} a_{mn}x_n + \bigwedge\limits_{n=1}^{2} u_{mn}g_n(\varrho_n(t-\tau)) + \bigvee\limits_{n=1}^{2} v_{mn}g_n(\varrho_n(t-\tau)) \\ \qquad\qquad + \bigwedge\limits_{n=1}^{2} \widehat{P}_{mn}x_n + \bigvee\limits_{n=1}^{2} \widehat{Q}_{mn}x_n + I_m, \\ \varrho_m(t) = \beta_m(t), t \in [-\tau, t_0], \end{cases} \tag{41}$$

where $b_1 = 0.2$, $b_2 = 0.1$, $\Delta b_1(t) = \Delta c_{1n}(t) = 0.1\cos t$, $\Delta b_2(t) = \Delta c_{2n}(t) = 0.1\sin t$, $h_n(\varrho) = g_n(\varrho) = \tanh(\varrho)$, $(c_{mn})_{2\times 2} = \begin{bmatrix} -1.2 & -2.0 \\ 0.8 & -1.4 \end{bmatrix}$, $(a_{mn})_{2\times 2} = \begin{bmatrix} 0.2 & 0.3 \\ 0.1 & 0.4 \end{bmatrix}$, $(\widehat{P}_{mn})_{2\times 2} = \begin{bmatrix} 0.1 & 0.3 \\ 0.3 & 0.1 \end{bmatrix}$, $(\widehat{Q}_{mn})_{2\times 2} = \begin{bmatrix} 0.3 & 0.2 \\ 0.4 & 0.1 \end{bmatrix}$, $(u_{mn})_{2\times 2} = \begin{bmatrix} -1.5 & -0.1 \\ -0.3 & -2.5 \end{bmatrix}$, $(v_{mn})_{2\times 2} = \begin{bmatrix} -0.8 & -0.1 \\ -0.2 & -1.5 \end{bmatrix}$, $(x_n) = \begin{bmatrix} 0.2 \\ 0.2 \end{bmatrix}$, *and* $I = \begin{bmatrix} 0 \\ 0 \end{bmatrix}$. *It is clear that Assumption 1 holds for* $\mathcal{L}_n^h = \mathcal{L}_n^g = 1$. *Based on master system (41), one can get the following slave system*

$$\begin{cases} {}_{t_0}^{c}\mathscr{D}_t^{0.92}\rho_m(t) = -(b_m + \Delta b_m(t))\rho_m(t) + \sum\limits_{n=1}^{2}(c_{mn} + \Delta c_{mn}(t))h_n(\rho_n(t)) \\ \qquad\qquad + \sum\limits_{n=1}^{2} a_{mn}x_n + \bigwedge\limits_{n=1}^{2} u_{mn}g_n(\rho_n(t-\tau)) + \bigvee\limits_{n=1}^{2} v_{mn}g_n(\rho_n(t-\tau)) \\ \qquad\qquad + \bigwedge\limits_{n=1}^{2} \widehat{P}_{mn}x_n + \bigvee\limits_{n=1}^{2} \widehat{Q}_{mn}x_n + I_m + \Theta_m(t), \\ \rho_m(t) = \gamma_m(t), t \in [-\tau, t_0], \end{cases} \tag{42}$$

where the network parameters are the same as (41).

Let parameters $t_0 = 0$, $\tau = 0.2$, $\kappa_1 = \kappa_2 = 1, \sigma = 0.12, \delta = 0.01, \varsigma^* = 3.7$, and $\chi = 4.3$. Simple calculations indicate that $\varsigma^* > \max_{1\le m\le k}\left[-b_m + \Xi_m + \sum\limits_{n=1}^{k}\Big(|c_{nm}| + \Pi_{nm}\Big)\mathcal{L}_m^h\right] = 3.6$, $\chi > \max_{1\le m\le k}\left[\sum\limits_{n=1}^{k}\Big(|u_{nm}| + |v_{nm}|\Big)\mathcal{L}_m^g\right] = 4.2$, $\phi = \min_{1\le m\le k}\left[b_m - \Xi_m - \sum\limits_{n=1}^{k}\Big(|c_{nm}| + \Pi_{nm}\Big)\mathcal{L}_m^h + \varsigma^*\right] = 0.1$, $\psi = -0.02$, $\underline{t} = 1.9384$, and $\bar{t} = 19.9698$. It is not difficult to find that all the inequality constraints in Theorem 2 are satisfied for the above parameters.

By the nonlinear controller (15), the time evolution of the adaptive control strength $\varsigma_m(t)$ is given in Figure 6. Figure 7 shows the system errors of different states under adaptive control schemes, and Figure 8 presents the corresponding norm of the system error. To quantify the variation in the error norm, the time evolution of $\|\epsilon(t)\|$ between systems (41) and (42) is given in Table 6. Obviously, with the advances in control, the controlled master and slave networks (41) and (42) can achieve FT Mittag–Leffler synchronization.

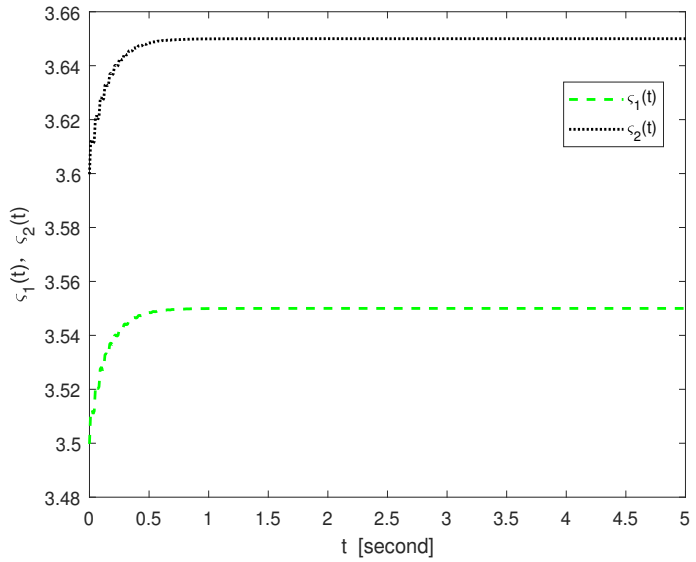

Figure 6. The time evolution of the control strength $\varsigma_m(t)$ in Example 2.

Table 6. The time evolution of the error norm $\|\epsilon(t)\|$ between UFODCNNs (41) and (42).

Time t	**0.2**	**0.3**	**0.4**	**0.5**	**0.6**	**0.7**	**0.8**
Error norm	0.0372	0.0243	0.0068	0.0037	0.0018	0.0005	0

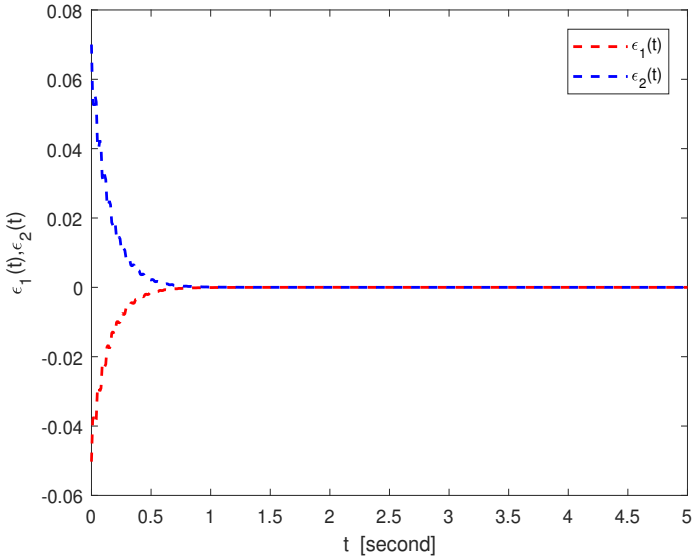

Figure 7. System errors $\epsilon_m(t)$ between fuzzy UFODCNNs (41) and (42) under adaptive controller (15) in Example 2.

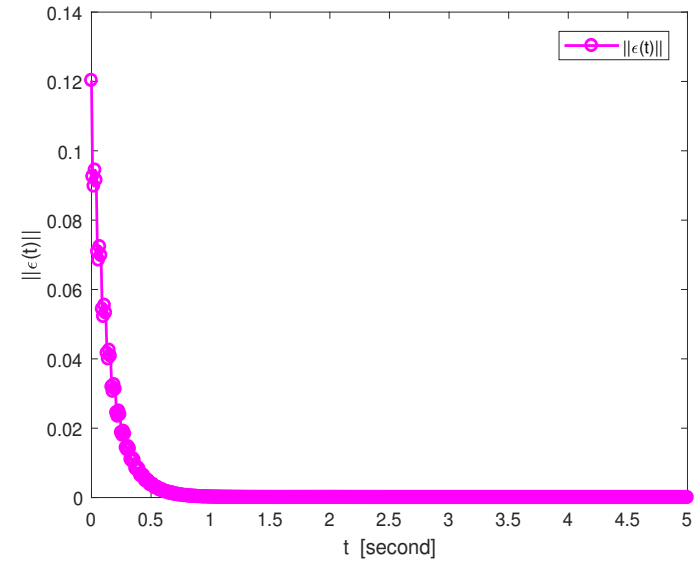

Figure 8. The norm of the system error between fuzzy UFODCNNs (41) and (42) under adaptive controller (15) in Example 2.

To evaluate the performance of our adaptive feedback controller, we compare the differences in the mean synchronization time and variance with nonlinear feedback controllers from the existing literature [16,51,52]. To ensure fairness in comparison, four feedback controllers are compared under the same system parameters. We randomly select the initial values $[-1, 1]$, and each control method is executed 10 times under the same initial conditions. As shown in Table 7, the performance of our adaptive controller in terms of the synchronization time and variance is superior to other controllers. From the perspective of the mean time, the cost time of our controller is 11.397% less than that of the second-ranked controller, and the variance of our controller is 12.5% less than that of the nonlinear feedback control in [51].

Table 7. Comparisons of mean time and variance with different control schemes.

Control Schemes	Mean Time	Variance
Nonlinear feedback control in [16]	0.857	0.021
Nonlinear feedback control in [51]	0.816	0.016
Simplified feedback control in [52]	0.945	0.018
Our adaptive feedback controller	0.723	0.014

Remark 10. *Noting the memory characteristics of fractional-order systems, this paper applies the Adams–Bashforth–Moulton approach in [33] to model the error evolution of delayed fractional-order nonlinear systems by MATLAB R2020b. The approach mainly consists of two phases: prediction and correction. First, the time intervals are divided using an equally spaced grid. The product rectangular rule and the series expansion are utilized to evaluate the prediction items. Second, the product trapezoidal quadrature rule is utilized to obtain the correction term. By combining the prediction and correction, the simulation examples can be realized.*

Remark 11. *In particular, the three modules in (15) show that* $\lim_{\epsilon_m(t)\to 0}\Theta_m(t)=\infty$. *In actual application, a bounded and smooth controller significantly reduces the control energy consumption. To avoid singularity, one can replace the* $-\chi\frac{\epsilon_m(t)}{|\epsilon_m(t)|}|\epsilon_m(t-\tau)|-\varsigma_m(t)\epsilon_m(t)-\delta\frac{\epsilon_m(t)}{|\epsilon_m(t)|}$ *with* $-\chi\frac{\epsilon_m(t)}{|\epsilon_m(t)|+\epsilon^\star}|\epsilon_m(t-\tau)|-\varsigma_m(t)\epsilon_m(t)-\delta\frac{\epsilon_m(t)}{|\epsilon_m(t)|+\epsilon^\star}$, *where* $\epsilon^\star>0$ *indicates a sufficiently small constant.*

Remark 12. *The synchronization results derived in this article have potential applications in the real world. In secure communication, the drive system hides encrypted information in chaotic signals for transmission, and the response system must accurately synchronize the chaotic dynamics of the transmission end to extract the original information. The FT synchronization control of neural networks can ensure that the receiving end completes synchronization within strict time constraints, greatly improving the real-time performance and anti-interception ability of communication. In multi-robot collaborative control, one robot (leader) serves as the driving system, while other robots (followers) serve as the responding systems, requiring consistent posture, speed, or trajectory with it. FT synchronization control can ensure that all robots reach a consistent state within a finite time, thereby improving the system's response speed and overall coordination to sudden instructions. In the smart grid distributed optimization process, FT synchronization control can force the output frequency and phase of all power nodes to achieve synchronization in a very short time. This can effectively prevent frequency fluctuations caused by slow synchronization and significantly improve the stability of the power grid in response to sudden load changes.*

5. Conclusions

The FT synchronization and FT Mittag–Leffler synchronization issues have been studied for the nonlinear UFODCNNs with multiple fuzzy operators. By combining the adaptive control mechanism, the fractional comparison theorem, and the fractional stability theory, novel synchronization conditions in finite time for the UFODCNNs were obtained. All conditions were in simple scalar inequality form, eliminating the need for the linear matrix inequality toolbox and reducing the computational burden. Two experiments validated the effectiveness of the synchronization results in this article. A future direction is to study the synchronized control of fractional-order neural networks under time-varying topologies or switching connection weights to improve the model's adaptability to real network dynamics. Another research direction is to explore the effect of variable-order derivatives on neural network dynamics to reveal the synchronization mechanism of adaptive regulation order.

Author Contributions: Conceptualization, K.S., H.F., and Z.G; Methodology, K.S., Z.G., and J.C; Software, H.F., J.C., and A.Z.; Writing—original draft, H.F., K.S., and Z.G.; Writing—review and editing, H.F., J.C., and A.Z. All authors have read and agreed to the published version of the manuscript.

Funding: The first author was partially supported by the Engineering Research Center for Big Data Application in Private Health Medicine of Fujian Universities, Putian University, under Grant (MKF202401), and the APC was funded by (MKF202401). The second author was partially supported by the Sichuan Science and Technology Program under Grants (25NSFSC2581, 2024NSFSC2056). The fifth author was partially supported by the Guizhou Provincial Basic Research Program (Natural Science) under grant Qiankehejichu-zk[2025] General 233, the Guizhou Provincial Science and Technology Projects under Grant Qiankehejichu-[2024] Youth 186, and the National Natural Science Foundation of China under Grant (62403157).

Data Availability Statement: Data are contained within the article.

Conflicts of Interest: The authors declare no conflicts of interest.

References

1. Ding, D.; Tang, Z.; Park, J.H.; Ji, Z.C. Quasi-bipartite synchronization of derivatively coupled complex dynamic networks: Memory-based self-triggered approach. *IEEE Trans. Syst. Man, Cybern. Syst.* **2024**, *54*, 1611–1621. [CrossRef]
2. Zhao, C.; Chen, Y.P.; Shi, K.B.; Zhang, L.; Nie, Y.J. A relaxed Lyapunov function lemma and genetic algorithm applying to time-delay systems. *Chaos Solitons Fractals* **2025**, *199*, 116687. [CrossRef]
3. Xiao, J.Y.; Li, Y.T. Deep analysis on MLSY for fractional-order higher-dimension-valued neural networks under the action of free quadratic coefficients. *Expert Syst. Appl.* **2026**, *298*, 129586.
4. Pham, H.; Warin, X. Mean-field neural networks: Learning mappings on Wasserstein space. *Neural Netw.* **2023**, *168*, 380–393. [CrossRef]
5. Ding, D.; Tang, Z.; Park, J.H.; Wang, Y.; Ji, Z.C. Dynamic self-triggered impulsive synchronization of complex networks with mismatched parameters and distributed delay. *IEEE Trans. Cybern.* **2023**, *53*, 887–899. [CrossRef] [PubMed]
6. Luo, R.F.; Ren, J.J.; Shi, K.B. Stability analysis of delayed T-S fuzzy power system via a cubic function negative determination lemma. *Nonlinear Dyn.* **2025**, *113*, 5439–5456. [CrossRef]
7. Fan, H.G.; Chen, X.J.; Shi, K.B.; Wen, H. Distributed delayed impulsive control for μ-synchronization of multi-link structure networks with bounded uncertainties and time-varying delays of unmeasured bounds: A novel Halanay impulsive inequality approach. *Chaos Solitons Fractals* **2024**, *186*, 115226. [CrossRef]
8. Han, T.Y.; Liang, Y.; Fan, W.J. Dynamics and soliton solutions of the perturbed Schrodinger-Hirota equation with cubic-quintic-septic nonlinearity in dispersive media. *Aims Math.* **2025**, *10*, 754–776. [CrossRef]
9. Zhang, K.; Cao, J.P.; Lyu, J.J. Dynamic behavior and modulation instability for a generalized nonlinear Schrodinger equation with nonlocal nonlinearity. *Phys. Scr.* **2025**, *100*, 015262. [CrossRef]
10. Tang, Z.; Xuan, D.L.; Park, J.H.; Wang, Y.; Feng, J.W. Impulsive effects based distributed synchronization of heterogeneous coupled neural networks. *IEEE Trans. Netw. Sci. Eng.* **2021**, *8*, 498–510. [CrossRef]
11. Cai, J.Y.; Yi, C.B.; Luo, X.; Xiao, C.R. Output feedback tracking consensus of switched stochastic uncertain multiagent systems via event-triggered control. *IEEE Syst. J.* **2024**, *308*, 130–141. [CrossRef]
12. Ding, K.; Zhu, Q.X. A note on sampled-data synchronization of memristor networks subject to actuator failures and two different activations. *IEEE Trans. Circuits Syst. II Express Briefs* **2021**, *68*, 2097–2101. [CrossRef]
13. Yi, C.B.; Cai, J.Y.; Guo, R. Synchronization of a class of nonlinear multiple neural networks with delays via a dynamic event-triggered impulsive control strategy. *Electron. Res. Arch.* **2024**, *32*, 4581–4603. [CrossRef]
14. Yao, W.; Wang, C.H.; Sun, Y.C.; Gong, S.Q.; Lin, H.R. Event-triggered control for robust exponential synchronization of inertial memristive neural networks under parameter disturbance. *Neural Netw.* **2023**, *164*, 67–80.
15. Sun, X.; Yang, Y.Q. Quasi-Mittag-Leffler projective synchronization of delayed chaotic fractional order neural network with mismatched parameters. *Fractal Fract.* **2025**, *9*, 379.
16. Fan, H.G.; Shi, K.B.; Guo, Z.Z.; Zhou, A.R. Finite-time synchronization criteria for Caputo fractional-order uncertain memristive neural networks with fuzzy operators and transmission delay under communication feedback. *Fractal Fract.* **2024**, *8*, 619.
17. Zhao, L.H.; Wen, S.P.; Xu, M.; Shi, K.B.; Zhu, S.; Huang, T.W. PID control for output synchronization of multiple output coupled complex networks. *IEEE Trans. Netw. Sci. Eng.* **2022**, *9*, 1553–1566. [CrossRef]
18. Liu, S.R.; Liu, X.W. Output synchronization and PID control for directed networks with multiple communications. *IEEE Trans. Syst. Man Cybern. Syst.* **2025**, *55*, 1620–1633.

19. Suid, M.H.; Ahmad, M.A. Optimal tuning of sigmoid PID controller using Nonlinear Sine Cosine Algorithm for the Automatic Voltage Regulator system. *ISA Trans.* **2022**, *128*, 265–286. [CrossRef]
20. Ghazali, M.R.; Ahmad, M.A.; Ismail, R.M.T.R. A multiple-node hormone regulation of neuroendocrine-PID (MnHR-NEPID) control for nonlinear MIMO systems. *IETE J. Res.* **2022**, *68*, 4476–4491.
21. Li, L. A novel optimization control of gas turbine based on a hybrid method using the BELBIC and adaptive multi input multi output feedback control. *J. Intell. Fuzzy Syst.* **2023**, *45*, 863–876. [CrossRef]
22. Huan, M.C.; Li, C.D. Synchronization of reaction-diffusion neural networks with sampled-data control via a new two-sided looped-functional. *Chaos Solitons Fractals* **2023**, *167*, 113059. [CrossRef]
23. Cui, Y.; Ge, X.H.; Cheng, P.; Liu, X. Resilient synchronization of interconnected dynamical networks with DoS attacks: An adaptive event-triggered control approach. *Neurocomputing* **2025**, *638*, 130192. [CrossRef]
24. Fan, H.G.; Rao, Y.; Shi, K.B.; Wen, H. Time-varying function matrix projection synchronization of Caputo fractional-order uncertain memristive neural networks with multiple delays via mixed open loop feedback control and impulsive control. *Fractal Fract.* **2024**, *8*, 301 [CrossRef]
25. Alsaedi, A.; Cao, J.D.; Ahmad, B.; Alshehri, A.; Tan, X.G. Synchronization of master-slave memristive neural networks via fuzzy output-based adaptive strategy. *Chaos Solitons Fractals* **2022**, *158*, 112095. [CrossRef]
26. Liu, F.; Song, Q.; Wen, G.H.; Cao, J.D.; Yang, X.S. Bipartite synchronization in coupled delayed neural networks under pinning control. *Neural Netw.* **2018**, *108*, 146–154. [CrossRef]
27. Zhang, X.Y.; Li, C.D.; Li, H.F.; Cao, Z.R. Synchronization of uncertain coupled neural networks with time-varying delay of unknown bound via distributed delayed impulsive control. *IEEE Trans. Neural Netw. Learn. Syst.* **2023**, *34*, 3624–3635. [CrossRef]
28. Hua, W.T.; Wang, Y.T.; Liu, C.Y. New method for global exponential synchronization of multi-link memristive neural networks with three kinds of time-varying delays. *Appl. Math. Comput.* **2024**, *471*, 128593. [CrossRef]
29. Wan, P.; Zhou, Y.F.; Zeng, Z.G. Adaptive drive-response synchronization of timescale-type neural networks with unbounded time-varying delays. *IEEE Trans. Neural Netw. Learn. Syst.* **2025**, *36*, 1056–1068. [CrossRef]
30. Zhang, Z.Y.; Wei, X.F.; Wang, S.Z.; Lin, C.; Chen, J. Fixed-time pinning common synchronization and adaptive synchronization for delayed quaternion-valued neural networks. *IEEE Trans. Neural Netw. Learn. Syst.* **2024**, *35*, 2276–2289. [CrossRef]
31. Podlubny, I. *Fractional Differential Equations*; Academic Press: New York, NY, USA, 1999.
32. Chen, B.S.; Chen, J.J. Global asymptotical ω-periodicity of a fractional-order non-autonomous neural networks. *Neural Netw.* **2015**, *68*, 78–88. [PubMed]
33. Bhalekar, S.; Gejji, V. A predictor-corrector scheme for solving nonlinear delay differential equations of fractional order. *J. Fract. Calc. Appl.* **2011**, *1*, 1–9.
34. Duan, L.; Wei, H.; Huang, L.H. Finite-time synchronization of delayed fuzzy cellular neural networks with discontinuous activations. *Fuzzy Sets and Systems* **2019**, *361*, 56–70. [CrossRef]
35. Yang, X.J.; Li, C.D.; Song, Q.K.; Chen, J.Y.; Huang, J.J. Global Mittag-Leffler stability and synchronization analysis of fractional-order quaternion-valued neural networks with linear threshold neurons. *Neural Networks* **2018**, *105*, 88–103. [CrossRef]
36. Peng, Q.; Lin, S.M.; Tan, M.C. Quantized hybrid impulsive control for finite-time synchronization of fractional-order uncertain multiplex networks with multiple time-varying delays. *Commun. Nonlinear Sci. Numer. Simul.* **2025**, *142*, 108540. [CrossRef]
37. Pan, H.H.; Huang, C.D.; Cao, J.D.; Liu, H. Global Mittag-Leffler synchronization of discontinuous memristor-based fractional-order fuzzy inertial neural networks with mixed delays. *Neurocomputing* **2025**, *626*, 129475. [CrossRef]
38. Xiao, J.Y.; Zhong, S.M.; Li, Y.T.; Xu, F. Finite-time Mittag-Leffler synchronization of fractional-order memristive BAM neural networks with time delays. *Neurocomputing* **2017**, *219*, 431–439. [CrossRef]
39. Popa, C.A.; Kaslik, E. Finite-time Mittag-Leffler synchronization of neutral-type fractional-order neural networks with leakage delay and time-varying delays. *Mathematics* **2020**, *8*, 1146.
40. Xiao, J.Y.; Cao, J.D.; Cheng, J.; Zhong, S.M.; Wen, S.P. Novel methods to finite-time Mittag-Leffler synchronization problem of fractional-order quaternion-valued neural networks. *Inf. Sci.* **2020**, *526*, 221–244.
41. Du, F.F.; Lu, J.G. Adaptive finite-time synchronization of fractional-order delayed fuzzy cellular neural networks. *Fuzzy Sets Syst.* **2023**, *466*, 108480.
42. Xu, Y.; Chen, Z.; Li, W.X.; Wu, Y.B. Exponential stability of fractional-order fuzzy multilayer networks with short memory and noninstantaneous impulses via intermittent control. *IEEE Trans. Fuzzy Syst.* **2025**, *33*, 1639–1649. [CrossRef]
43. Su, Y.; Hu, C.; Yu, J.; Wen, S.P.; Li, H.L. Bipartite output synchronization of fuzzy fractional output-coupled networks via membership function-dependent adaptive control. *IEEE Trans. Autom. Sci. Eng.* **2025**, *22*, 14147–14157.
44. Zhang, H.M.; Yin, X.N.; Zhang, H.; Zhang, W.W. Global Mittag-Leffler lag projective synchronization for Caputo-type delayed Cohen-Grossberg fuzzy neural networks. *Int. J. Control Autom. Syst.* **2025**, *23*, 212–222. [CrossRef]
45. Li, R.X.; Cao, J.D. Stabilization and synchronization control of quaternion-valued fuzzy memristive neural networks: Nonlinear scalarization approach. *Fuzzy Sets Syst.* **2024**, *477*, 108832. [CrossRef]

46. Li, H.L.; Cao, J.D.; Hu, C.; Zhang, L.; Jiang, H.J. Adaptive control-based synchronization of discrete-time fractional-order fuzzy neural networks with time-varying delays. *Neural Netw.* **2023**, *168*, 59–73. [CrossRef]
47. Li, H.L.; Cao, J.D.; Hu, C.; Jiang, H.J.; Alsaedi, A. Synchronization analysis of nabla fractional-order fuzzy neural networks with time delays via nonlinear feedback control. *Fuzzy Sets Syst.* **2024**, *475*, 108750. [CrossRef]
48. Zhao, F.; Jian, J.G.; Wang, B.X. Finite-time synchronization of fractional-order delayed memristive fuzzy neural networks. *Fuzzy Sets Syst.* **2023**, *467*, 108578. [CrossRef]
49. Ansari, M.S.H.; Malik, M. Projective synchronization of fractional order quaternion valued uncertain neural networks. *Chin. J. Phys.* **2024**, *88*, 740–755. [CrossRef]
50. Chen, R.; Li, H.L.; Liu, H.; Jiang, H.J.; Cao, J.D. Complete synchronization of discrete-time fractional-order T-S fuzzy complex-valued neural networks with time delays and uncertainties. *IEEE Trans. Fuzzy Syst.* **2025**, *33*, 842–856. [CrossRef]
51. Du, F.F.; Luo, J.G. Finite-time synchronization of fractional-order delayed fuzzy cellar neural networks with parameter uncertainties. *IEEE Trans. Fuzzy Syst.* **2023**, *31*, 1769–1779. [CrossRef]
52. Fan, H.G.; Chen, X.J.; Shi, K.B.; Liang, Y.H.; Wang, Y.; Wen, H. Mittag-Leffler synchronization in finite time for uncertain fractional-order multi-delayed memristive neural networks with time-varying perturbations via information feedback. *Fractal Fract.* **2024**, *8*, 422. [CrossRef]